Composite Structures 305 (2023) 116508

Contents lists available at ScienceDirect

Composite Structures

journal homepage: www.elsevier.com/locate/compstruct

A contactless characterization of CNT/Epoxy nanocomposites behavior under acid exposure

S. Tamayo-Vegas [a,*], K. Lafdi [a,b], M. Elsdon [c]

[a] Department of Mechanical Engineering, Northumbria University, United Kingdom
[b] Department of Chemical Engineering, University of Dayton, OH, United States
[c] Smart Materials and Surfaces Laboratory, Northumbria University, United Kingdom

ARTICLE INFO

Keywords:
Polymer nanocomposites
Carbon nanotubes
Wireless
Contactless Material Characterization
Acid Attack
Computational Modelling

ABSTRACT

The use of polymer nanocomposites is ubiquitous in every industry. The high corrosion resistance and chemical durability of CNT/Epoxy nanocomposites make them suitable for chemical plants, oil industries, and hydrogen storage. However, unexpected failures have been reported for chemicals that unavoidably penetrate, provoking deterioration and degradation of the composite constituents. Conventional methods are impractical for evaluating structural health conditions because they often require disassembly of the structure and complex post-processing analysis. Contactless material characterization methods, on the other hand, are rather promising tools. Nevertheless, the influence of nanofillers and acid attack diffusion on wireless signals has yet to be explored. In this study, the effects of acid attack periods (i.e. one, week, two weeks, and month) on the scattering parameters of microstrip antennas were investigated using a vector network analys. Additionally, an idealised multi-scale modelling approach was developed to study the influence of electrical conductivity and porosity volume changes on return loss (S11). The data showed that the diffusion of ions altered the specimen properties as time progressed. The increment in the electrical conductivity and porosity volume is reflected especially during the month-long period. Finally, in this study, it was found that wireless methods can be implemented to characterise materials which are beneficial for real-time in-situ structural health monitoring.

1. Introduction

In past decades, the industry of composite materials has faced steady growth with limitless applications. This continuous advancement in technology has resulted in a constant demand for multifunctional smart materials. Neat materials often lack this combination of features, thus failing to meet demands. Conversely, polymer composites possess remarkable characteristics. They exhibit, for instance, a high strength-to-weight ratio, fatigue resistance, high stiffness, and they are easy to manufacture. These qualities are beneficial for many industrial applications such as construction, aerospace, electronics, medicine, and sports. The improvements range from lightweight structures to enhanced mechanical, electrical, and thermal performance [1–10].

The polymer-based composites are also used in chemical plants, oil facilities, and hydrogen storage [11]. High corrosion resistance and chemical durability are imperative characteristics to withstand saline, corrosive and aggressive acids. Although polymer composite provides a high corrosion barrier and durability, unexpected structural failure before the designed service lifetime has been reported [12–14]. Direct contact with chemicals provokes unavoidable diffusion phenomena. Swelling, hydrolysis, hygroscopic dimensional changes, degradation and bleaching are responsible for causing structural deterioration and in many cases catastrophic failure. For instance, the matrix starts to swell and subsequently the reinforcements degrade [15,16]. To identify and mitigate failure, structural health monitoring (SHM) techniques are deployed to evaluate the structural condition. Usually, SHM employs the implementation of sensors and actuators, however, chemical storage facilities often evaluate the structural health with weight and volume measurements, and colour-based methods [14,17–19]. Although these methods can reasonably predict the structural state, they are mostly used post-use and impractical, as they require disassembly of the structure and complex machinery, resulting in time-consuming and expensive approaches.

In past years, as more powerful computers have been made available, contactless methods have been widely investigated. For instance, imaging-based methods such as laser measurements and wireless

* Corresponding author.
E-mail address: w18002002@northumbria.ac.uk (S. Tamayo-Vegas).

https://doi.org/10.1016/j.compstruct.2022.116508
Received 1 September 2022; Received in revised form 15 November 2022; Accepted 20 November 2022
Available online 2 December 2022

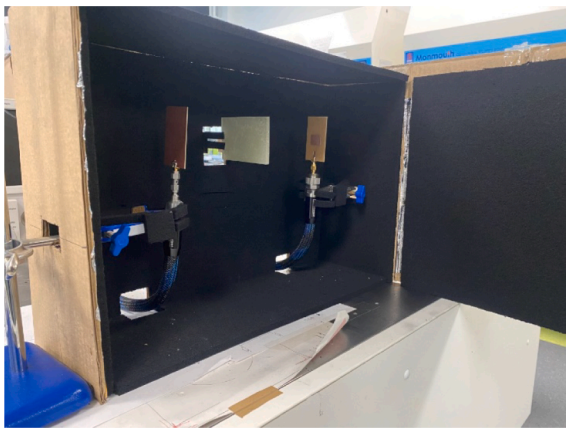

Fig. 1. Experimental Setup.

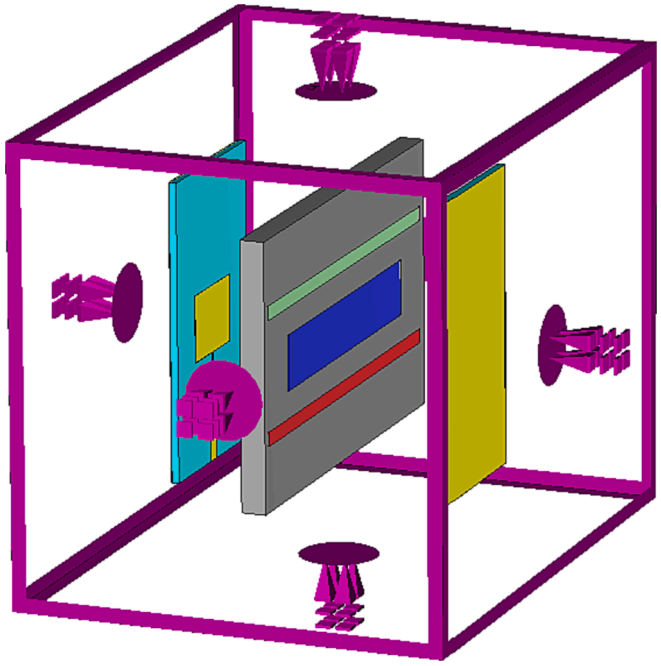

Fig. 2. Numerical Simulations Set-up.

communications, among others, benefit from powerful algorithms i.e. artificial intelligence, neural networks, and machine learning [19]. Although observation-based methods are powerful techniques, they are restricted to chemical storage applications. Wireless sensor technologies, on the other hand, are rather promising tools. The rapid advancement of technologies such as Bluetooth, RFID, ZigBee and NFC is allowing the implementation of wireless embedded sensors for SHM [20–23]. Nevertheless, not all of the aforenamed technologies are suitable for chemical diffusion sensing. For instance, placing Bluetooth chips, active RFID tags or ZigBee systems will need extra design and create additional stress areas [16,24–26]. On the other hand, chipless technologies such as passive RFID and NFC could be potentially deployed in chemical facilities [27–31]. The implementation of RFID technologies as a means of sensing has seen increasing use in food safety [32–39], environmental pollution [40–44], healthcare [45–49] and SHM applications [50–54]. The tags are modified or entirely constructed with composite materials. The materials are tuned for selectivity and sense the wanted phenomena.

Although the advancement is encouraging, in chemical and aggressive environments there have been reported few applications where RFID tags have been implemented. Mainly because the behaviours of composite materials under acid attack and the influence on the wireless signal have yet to be explored. Dielectric material characterization is often measured using Vector Network Analyzer using probes, waveguides, and antennas [18,29,53,55]. Wireless characterization could be obtained through the employment of horn antennas, helical antennas, and patch antennas. Horn antennas have been widely employed as they possess a wide bandwidth, allowing them to characterize through a large range of frequencies, however, this type of antenna regularly struggles to identify alterations. Patch antennas, on the other hand, are easy to construct and can be tailored to any frequency. Moreover, they naturally have narrow bandwidth that could be beneficial to measure the small changes that acid ions produce in signals. The most studied and simple parameters are scattering parameters, from which the dielectric properties can be derived [56–61].

In this study, the effects of acid diffusion at different time-scales was investigated using a contactless approach. Consequently, the nanocomposite samples were characterized using a Vector Network Analyzer and two microstrip antennas inside an anechoic chamber in the frequency range 3–6 GHz. First, two microstrip antennas with a resonance frequency of 5 GHz were designed. Separate samples were immersed in acid solution for four different periods of time (zero days, one week, two weeks, and one month). The samples were placed 25 mm from the transmission and receiving antennas. The antenna scattering parameters were obtained (return loss and insertion loss) and compared. Additionally, a multi-scale numerical approach was employed to investigate the potential effects of porosity and electrical conductivity variation in the scattering parameters. The results showed that as the percentage of carbon nanotubes in the sample increased, the ion diffusion rate decreased. Moreover, the diffusion caused an increase in the electrical conductivity and porosity. This was observed after one month of acid exposure. The numerical approach allowed the investigation of complex phenomena by altering the porosity and electrical conductivity. These changes are reflected wirelessly, which is beneficial for ubiquitous sensing.

2. Materials and methods

2.1. Materials and samples preparation

In this study, thirty-six specimens were utilized. The sample constituents were Multiwall Carbon Nanotubes (MWCNT) and Epoxy EPON 862. The specimens contain carbon nanotube (CNTs) fractions of 0 %, 0.5 %, 1 %, 2 %, 4 %, and 5 %. MWCNT diameter and length ranged from 30 μm to 100 μm and 20 nm to 100 nm, respectively. The specimens were fabricated through a process of shear mixing the CNTs in an ultrasonic bath in acetone for a period of one hour. Afterwards, while constantly mixing, epoxy resin was added until the solvent had evaporated. Finally, the mixture was poured into a silicone mould and hot-pressed in vacuum. The sample's dimensions were 80 mm in width, 52 mm in length, and 6 mm thick.

Subsequently, eighteen samples were immersed in a solution of sulfuric acid (H_2SO_4). The acid attack time was divided into three groups: one week, two weeks, and a month. Six samples were used for each timeline. The remaining eighteen were kept in normal conditions as control samples for the measurements.

2.2. Experimental procedure

The microwave materials characterization was performed using a Network Analyzer Agilent N230A at room temperature (25 °C). Two 85131F Flexible cables were connected to port 1 and port 2. The calibration was performed using the E-Calibration Kit N4693-60003. The free space measurements were performed using two patch antennas with a central resonance frequency of 5 GHz. Because the beamwidth of the antenna at the main lobe is three times less than the minimum transverse

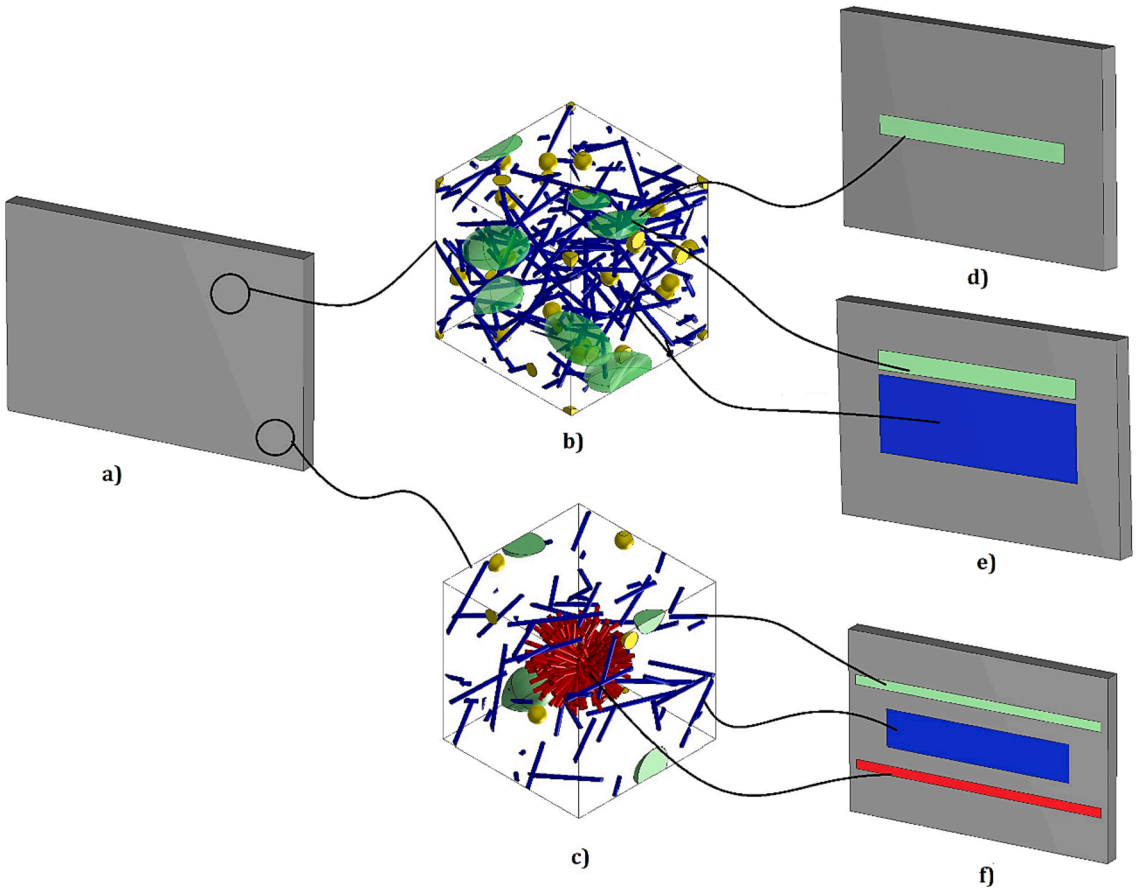

Fig. 3. Multi-scale Modelling CST. a) Sample a 1:1 scale. b) RVE with Carbon Nanotubes (Blue), Acid Ions (Yellow), Porous (Green). c) RVE with Carbon Nanotubes (Blue), Carbon Nanotubes Agglomeration (Red), Acid Ions (Yellow), Porous (Green). d) Sample at 1:1 scale with Porous Area for samples Epoxy, 0.05 wt% and 1%. e) Sample at 1:1 scale with Carbon nanotubes Networks for Sample 2 wt%. f) Sample at scale 1:1 with Carbon nanotube networks, and Carbon Nanotubes Agglomeration for Samples 4 wt% and 5 wt%. (For interpretation of the references to colour in this figure legend, the reader is referred to the web version of this article.)

Table 1
Samples Electrical conductivity (S/m) values.

Samples CNT %	*Electrical conductivity (S/m)*
0 wt%	2.123×10^{-5}
0.5 wt%	2.123×10^{-3}
1 wt%	5.195×10^{-2}
2 wt%	25
4 wt%	350
5 wt%	550

dimension of the sample, the diffraction effect at the edges of the samples were negligible [56].

The measurements were performed in the far-field range at frequency range 3 GHz to 6 GHz. First, the return loss (S11) and insertion loss (S21) of the antenna were obtained in free space inside the anechoic chamber. Then, after placing the samples in between the antennas at a distance of 25 mm, the scattering parameters were measured (see Fig. 1).

2.3. Numerical procedure

A numerical model of the scattering parameter was created using CST Studio Suite following the experimental conditions. The dimensions of the samples, along with the distance from antennas to the samples were set up as described in the experimental section. The boundary conditions were set to open added space to simulate the anechoic chamber as shown in Fig. 2. The sample construction, however, was done through a multiscale-modelling as shown in Fig. 3. The modelling approach follows the micromechanics theory where a representative volume element (RVE) is created to calculate the final properties of the nanocomposite. However, as RVEs are not supported in CST Studio Suite, we proposed a breakdown approach to model the constituents of the samples. The sample shown in Fig. 3a), at the nano scale, is formed by its elemental constituents: matrix, carbon nanotubes, porosity, and penetration of acid ions. Fig. 3b) and Fig. 3c) represent two RVE containing carbon nanotubes as blue cylindrical aggregates, porosity as a green sphere shape, penetration of ions as yellow spheres, and potential formation of carbon nanotubes agglomeration in red. These two RVE are the volume constituents for the three models. The models were divided according to previous studies in Table 1 [5,62] where it was demonstrated that the electrical percolation threshold (EPT) is achieved at 2 wt %. Moreover, above this percentage, the formation of agglomeration, although beneficial for electrical conductivity, produces porosity surrounding these bundles. Thus, for this purpose, Fig. 3d) was the model chosen before EPT (plain epoxy, 0.5 wt% and 1 wt%). The percolation model (2 wt%) is represented by Fig. 3e) where the extra formation of CNT is taken into account as the networks are formed. Finally, Fig. 3f) represents the model chosen for 4 wt% and 5 wt% where the porosity generated by the agglomerates was also modelled. The modelling followed the study of the influence of the acid penetration on the electrical conductivity of the sample, the dielectric property, and the volume of porosity generated.

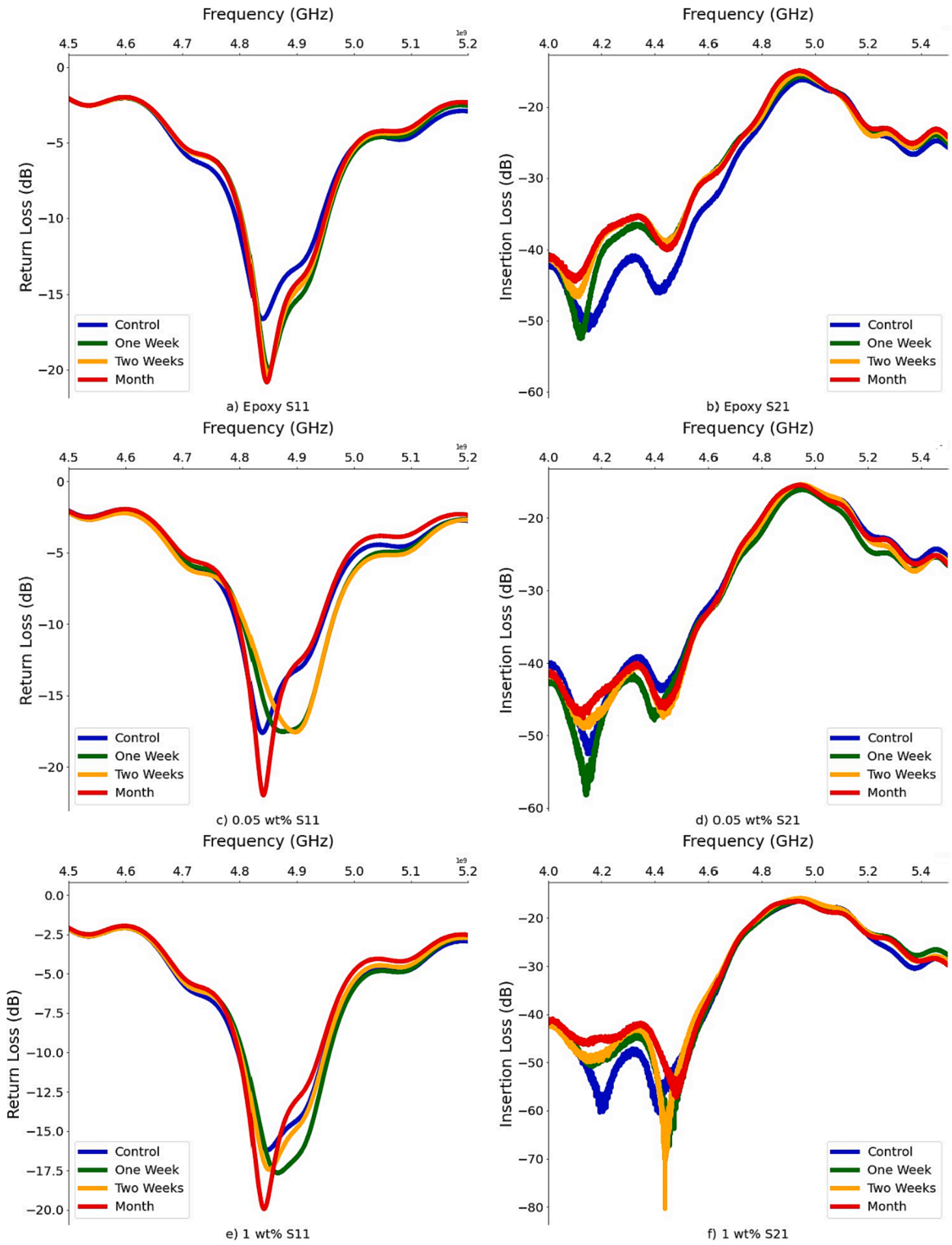

Fig. 4. Scattering parameters experimental results before electrical percolation threshold a) Epoxy S11. b) Epoxy S21. c) 0.5 wt% S11 d) 0.5 wt% S21 e) 1 wt% S11 f) 1 wt% S21.

3. Results and discussion

In this section, the experimental and numerical results are presented. This section opens with the experimental results separated into two parts, before and after electrical percolation threshold (EPT). The sample scattering parameters are presented throughout the curve profiles of control and acid exposure: one week, two weeks, and month. Subsequently, the modelling results are discussed following the same approach.

Fig. 4 shows the scattering parameters, return loss (S11) and insertion loss (S21) before EPT. The control samples' curve profiles are compared with the acid attack samples. In Fig. 4a) and 4b) the pristine epoxy experimental results are shown. At the resonance frequency, the S11 value reaches −16.637 dB, which gradually decreases with increasing acid exposure. The lack of reinforcements allows acid ions to penetrate the surface as early as one week. This phenomenon is

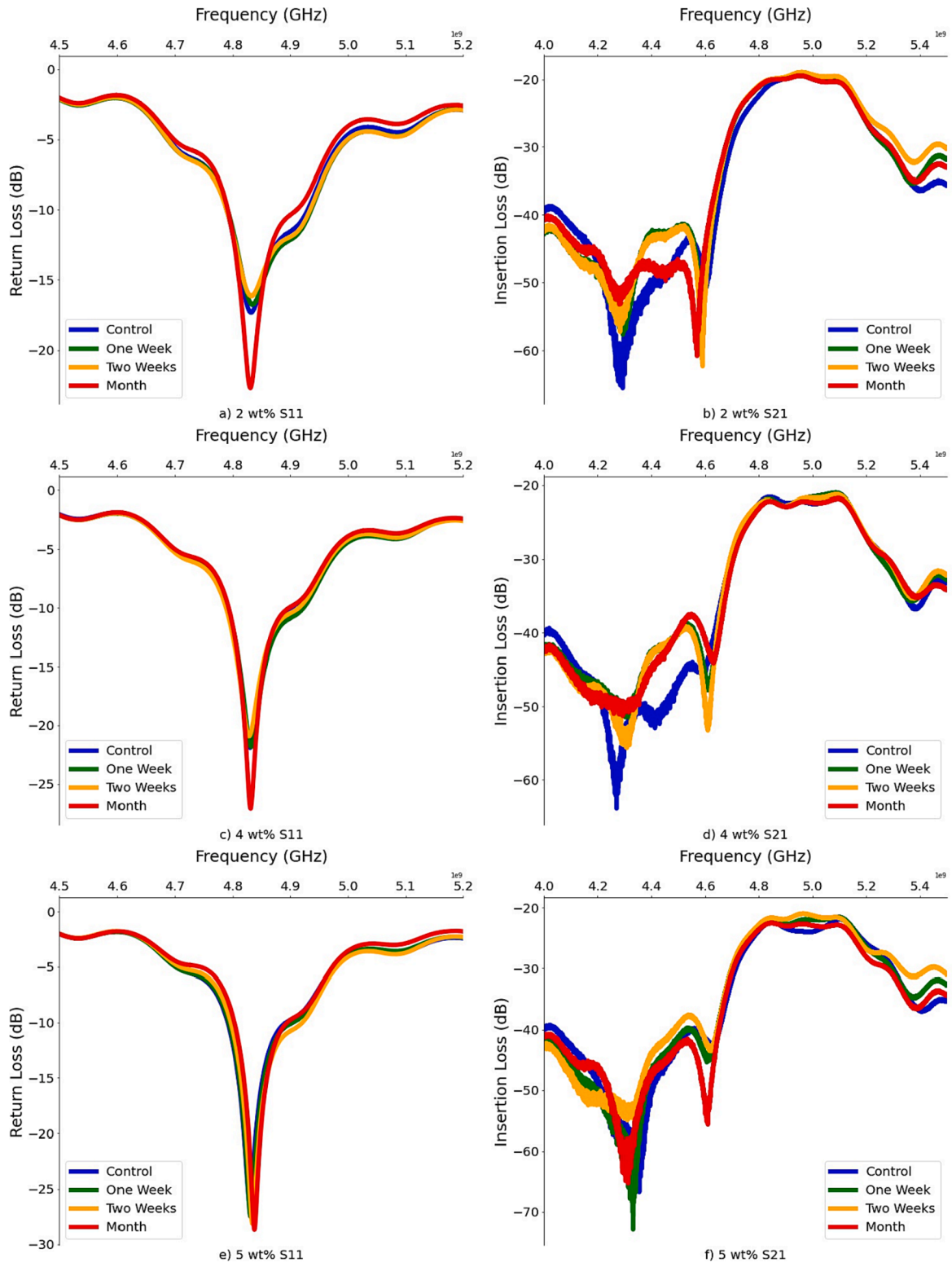

Fig. 5. Scattering parameters experimental results after electrical percolation threshold a) 2 wt% S11. b) 2 wt% S21. c) 4 wt% S11 d) 4 wt% S21 e) 5 wt% S11 f) 5 wt % S21.

validated with S11 values. The corresponding values appear to go along a decreasing pattern, jumping from −16.63762 dB (control sample) to −19.96 dB (one week), −20.27816 (two weeks), and −20.81702 dB (month). Although there is a marginal difference between samples that were exposed to the acid, there is a distinctive variation between the control samples and the samples exposed to acid.

The effects of acid attack are also found in insertion loss (Fig. 4b)). The distinctive behaviour can be observed in the frequency range of 4 GHz to 4.7 GHz. For instance, at 4.1 GHz, the control sample presents its lowest value of – 50 dB, similar to one week reaching approximately −50 dB. Nevertheless, the two week and one month samples increment to −45 dB and −43 dB respectively. Additionally, from 4.2 GHz to 4.6

Table 2
Return Loss values at resonance frequencies, experimental and simulations.

	Epoxy		**0.05 %**		**1 %**	
	Experimental	***Simulations***	***Experimental***	***Simulations***	***Experimental***	***Simulations***
Control	−16.63762	−15.74	−17.60299	−16.5283	−16.2089	−16.9989
One Week	−19.96565	−19.6895	−17.53416	−18.471	−17.66639	−17.5798
Two Weeks	−20.27816	−20.57	−17.5591	−18.470	−17.44843	−17.7009
Month	−20.81702	20.152	−21.97871	−21.3325	−19.94184	−19.8978
	2 %		**4 %**		**5 %**	
	Experimental	***Simulations***	***Experimental***	***Simulations***	***Experimental***	***Simulations***
Control	−17.33821	−16.3516	−21.89763	−20.7306	−26.27015	−26.063
One Week	−16.77927	−16.7388	−21.82417	−21.6882	−27.47799	−26.6777
Two Weeks	−16.17657	−17.0696	−20.9213	–22.0837	−28.12367	−26.9079
Month	–22.70312	–22.7943	−27.09709	−26.9079	−28.65134	–32.0255

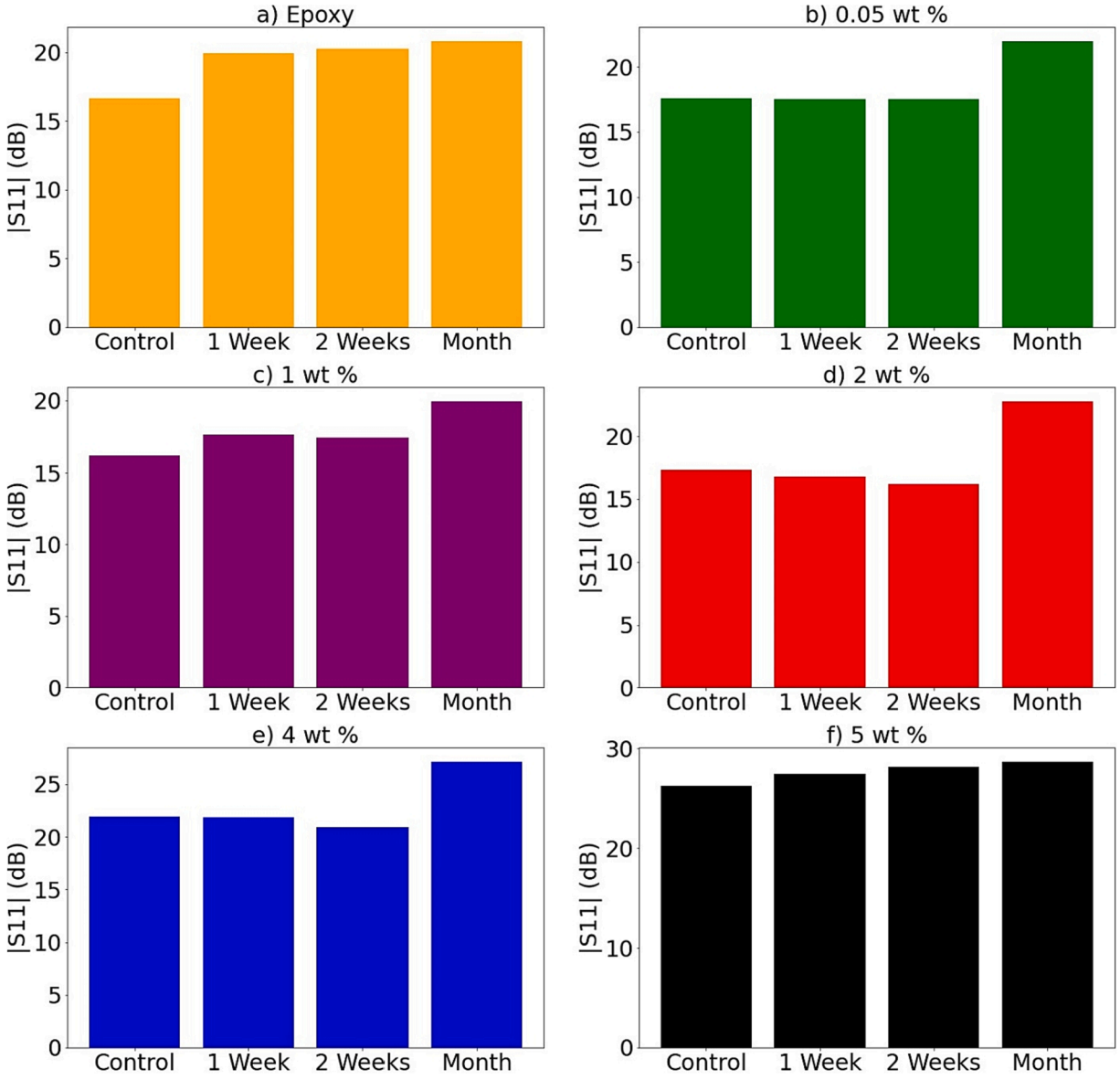

Fig. 6. S11 Absolute values at the resonance frequency.

Table 3
Modelling data Models before Electrical Percolation Threshold.

Sample	*Model*	*Conductivity (S/m)*	*Porosity Volume %*	*|S11| Simulations*
Epoxy	A	2.00E-05	0.72 %	15.737
	B	2.00E-05	0.80 %	19.68
	C	2.00E-05	1.63 %	20.58
	D	2.00E-05	2.20 %	20.15
0.05 %	A	2.00E-03	0.38 %	16.5
	B	2.80E-03	0.79 %	18.47
	C	3.10E-03	0.79 %	18.47
	D	4.00E-03	0.90 %	21.34
1 %	A	2.00E-02	0.36 %	16.998
	B	3.20E-02	0.65 %	17.58
	C	3.80E-02	0.95 %	17.7
	D	4.00E-02	1.72 %	19.89

GHz the three acid samples fluctuate above the control sample. The latter does not reach −40 dB, whereas the acid samples oscillate up to −35 dB.

Fig. 4c) and 4d) depict the scattering parameters of the first nanocomposite sample containing 0.05 wt% of CNT. At the resonance frequency, the control sample presents its lowest S11 value of −17.609 dB. Although one and two weeks generate comparable results of −17.534 dB and −17.555 dB respectively, the central resonance frequencies increase from 4.8 GHz to 4.9 GHz. In addition, the month acid attack sample gives the largest decrease in terms of resonance frequency, reaching −21.978 dB. This observation reveals that a small percentage of carbon nanotubes delay the diffusion of acid within the first weeks. The acid's effect on the nanocomposite is also consistent with the S21 parameter (Fig. 4d)), particularly in the frequency range 4 GHz to 4.2 GHz. Two weeks and one month present higher values than the control sample and one week. However, at greater frequencies, the four samples have shown equivalent results.

Fig. 4e) and Fig. 4f) depict the scattering parameters of the sample containing 1 wt%. At this percentage, the control sample shows the highest value of −16.208 dB, thereafter the acid attack provokes a steady decrease. The declining trend starts with one week at −17.666 dB moving to −17.448 dB at two weeks. The same influence, yet the largest, was found at one month of acid exposure: −19.941 dB. It is worth mentioning that the one and two week samples have similar results; a small, yet distinct variation from the control sample. Similar to previous samples, in the frequency region 4 GHz to 4.5 GHz (Fig. 4f)), the effects of the acid attack are noticed through the increase of the values in comparison to the control sample.

Fig. 5 depicts the samples' scattering parameters after EPT (2 wt%, 4 wt% and 5 wt%). At these percentages of nanofiller, it was found that in the first two weeks of acid exposure, there is marginal variation. Moreover, at 5 wt% the four samples presented minimal decremental variation. However, 2 wt% and 4 wt% present the largest difference between the control and one month samples. For instance, the largest difference between a control sample and an acid attack sample is found at 2 wt% with the one month exposure time. The control sample reached a value of −17.338 dB, whereas the one month acid sample decreases to as low as –22.703 dB. On the contrary, the one and two week samples showed comparable values of −16.779 dB and −16.176 dB respectively. One possible explanation is that as the volume of carbon nanotubes increases, the acid diffusion is delayed, thus minimizing the impacts of acid attack. This phenomenon is clearly depicted in Fig. 5a), where the red profile curve is distinctive from that of the other samples (control, one week, and two weeks). On the insertion loss, depicted in Fig. 5b), is also found that the region of acid attack influence is from 4 GHz to 4.5 GHz.

In the same manner, as the CNT percentage increases up to 4 wt%, the diffusion of acid ions faces a greater resistance. The value comparison between the control and one and two week samples is almost negligible. Nevertheless, as expected, as time passes, the alteration is quite evident in the one month sample. At this percentage, the difference is approximately 5 dB and the value reaches as low as −27.09 dB (Fig. 5c)). This trend was observed in Fig. 5d). In this case, however, all the acid time frames present a distinctive behaviour. In contrast with the previous samples, the range of frequencies seems to shrink, and the influence is just evident in a small frequency window from 4.4 GHz to 4.6 GHz.

Finally, the sample containing 5 wt% is presented in Fig. 5e) and 5f) for the return loss and insertion loss respectively. At this high concentration of CNT, the acid attack at all time frames is less evident. As can be seen in Fig. 5e) and Fig. 5f) the four profile curves follow almost an identical path. The effects of the acid ions just change a few units at the resonance frequency. Although the difference is minimal, the trend seems to be negative from −26.270 dB, −27.477 dB, − 28.123 dB to −28.651 dB. Nonetheless, this small difference could be related to the difference between the samples and the common artifact of the measurement technique and not the acid attack.

Table 2 resumes the values of the experimental and simulations at the resonance frequencies from all the samples at the control and acid attack. These values can clearly indicate the influence of the acid attack as we have been discussing. In addition, the simulation results are compared in this table, showing a good correlation of the multiscale modelling. An extended discussion is found in the next paragraphs.

A graphical representation is depicted in Fig. 6. A clear distinction is always found during the month attack. However, the different percentage of nanofillers indicates distinctive behaviour under acid attack. For instance, pristine epoxy shows the impact as early as one week and these phenomena are kept distinct in the following time frames. Distinctively, the nanocomposite containing 0.5 wt%, 1 wt% 2 wt% and 4 wt% only showed clear effects at month attack. Additionally, after the percolation threshold (i.e. 2 wt% and 4 wt%), the largest difference is found between control and month of acid attack. The composite containing 5 wt% showed marginal variations as can be been in Fig. 6 f).

Table 3 shows the parameters data for the models before the electrical percolation threshold. In the control samples, the conductivity is set according to Table 1. The dielectric values come from the Epoxy data sheet. As the dielectric also follows a percolation threshold, we assumed that at a low percentage of carbon nanotubes, the dielectric bulk value will be the same as plain Epoxy. Following the models for the epoxy, the electrical conductivity was set to not vary as the acid attack penetrates the material, thus only the porosity was assumed to vary.

These models are compared in Fig. 7. In each figure, the experimental and simulation results are compared. For illustration purposes, the control samples along with the one week and two week samples are compared in Fig. 7a) and one month in Fig. 7b). Fig. 7 a) and b) represent the Epoxy sample experimental and simulation results. Following the experimental results, the acid epoxy samples showed variation as early as one week. In the plain epoxy simulations, small percentage of porosity was considered at 0.72 %, this value was set to increase as time passed. As soon as porosity value increased, the software showed a large decrease of S11. As was expected, the acid ions degraded and formed porousities within the material. The model continued to follow the decreasing trend, increasing the percentage of porosity generated as time passed. These values are not absolute but rather a comparison and exemplification of how porosity influences S11.

For the nanocomposites, a different approach was followed. First, the electrical conductivity of the control sample was set according to previous work (Table 1). Second, the dielectric was set to be approximately the same as plain epoxy. For the acid samples, it was assumed that as the ions penetrate and start to diffuse, they change the electrical properties of the sample. This is because the ions influence the formation of carbon nanotube networks. Thus we set to augment in a slightly yet incremental pattern. The porosity also was set to increase as the acid exposure time increased.

Fig. 7 c) and Fig. 7 d) represent the nanocomposite with 0.5 wt%. The variation among control and acid samples was numerically obtained by

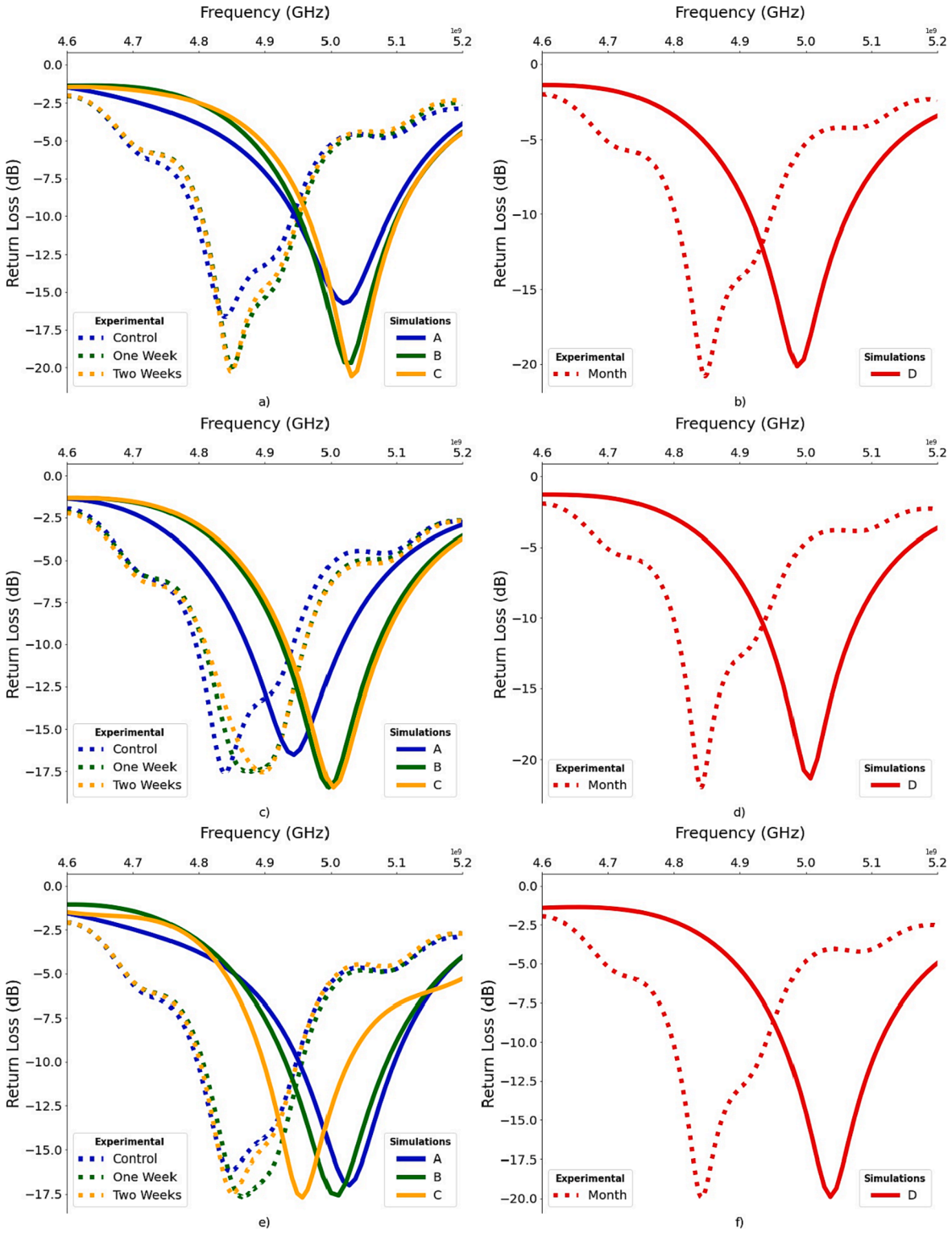

Fig. 7. Comparison of S11 curve experimental and numerical results before electrical percolation threshold a) Epoxy-one and two weeks. B) Epoxy month. C) 0.5 wt % one and two weeks d) 0.5 wt% month e) 1 wt% one and two weeks f) 1 wt% month.

Table 4
Modelling data after percolation threshold.

Sample	*Model*	*Conductivity (S/m)*	*Agglomeration Volume*	*Porosity Volume*	*|S11| Simulation*
2	A	25	–	4.25 %	16.3516
	B	25		4.93 %	16.7388
	C	30		5.44 %	17.0696
	D	30		4.96 %	22.7943
4	A	450	6 %	3.4 %	20.7306
	B	450		3.96 %	21.6882
	C	450		4.62 %	22.0837
	D	750		6.28 %	26.9079
5	A	550	7 %	7 %	26.063
	B	750		9.45 %	26.6777
	C	550		10.03 %	26.9079
	D	600		10.03 %	32.0255

varying the electrical conductivity and the porosity. The one week and two week samples had the same value of porosity, however, the conductivity was set to slightly increase. The results matched the experimental results and the switch or resonance frequency was seen experimentally and numerically with these small changes. The one month long exposure was slightly increased in the numerical parameters yet the conductivity doubled obtaining a perfect match with the experimental results.

For the 1 wt%, it was observed that experimentally, the two-week exposure presented a decreased central resonance frequency. For this, the numerical approach was set to slightly increase the porosity. The same phenomenon was observed with model C. The minimum values were obtained when the porosity was the highest and the electrical conductivity was higher, thus the acid provoked both phenomena, especially after one month of exposure.

The modelling of the acid penetration in nanocomposites is a very complex phenomenon. Especially after the percolation threshold, where another phenomenon—the tunnelling effect—affects the electrical behaviour of the nanocomposite. With randomly distributed nanotubes, the network properties formed within the sample are complex to predict. Another consideration is that at high concentrations the unavoidable formation of agglomeration directly influences the properties. These agglomerates can potentially increase the electrical conductivity, and also deliver a tougher path for acid diffusion. The increase of the electrical conductivity, therefore, is not the only phenomenon occurring within the diffusion of acid. The generation of porosity is undoubtedly a factor and is fortunately reflected in the experimental and simulation approaches.

In Table 4, the model parameters after the percolation threshold are presented. According to previous study (only at 4 and 5 wt%) [62], the agglomerations affect the mechanical properties which could mean that only at this percentage the formation reaches an influenceable percentage where the properties could be altered.

The wireless measurement is an extremely complex phenomenon to model. However, the variation of the conductivity and the variation of porosity as time passes can deliver an insightful understanding of the phenomena that occur with the diffusion of acid. Fig. 8 depicts the models compared with the experimental data. As can be seen, the models behave similarly to the measurement with the VNA. The porosity values shown in Table 4, are not strictly definite, rather a representative number to understand the increment and the influence on the return loss of the sample. Additionally, the conductivity values, while perhaps not definitive, potentially describe the complex phenomena that occur in the values within electrical resistance in disordered media.

Fig. 8 represents the models after the percolation threshold was achieved compared with experimental results. At the percolation threshold, numerically the curves of the acid attack follow a close path. This is obtained with the slight increase in electrical conductivity and formation of porosity. Fig. 8a) and Figure b) also show how the bandwidth of the sample at one month of exposure gets smaller. These phenomena are also seen at 4 and 5 wt% experimentally and numerically (Fig. 8 d) and Fig. 8 f)). With these last two nanocomposites, the generation of porosity is bigger. Even though the CNT could help to stop the penetration of acid, the agglomeration has been proved to form porosity surrounding these areas. Additionally, the electrical conductivity was increased at this porosity, however, especially at high percentages such as 5 wt%, the difference between acid and normal conditions is less evident. At this high percentage, the difference could be strictly related to the formation of networks and the distribution of agglomerates. Also, as the percolation threshold has already occurred, the potential increase in conductivity caused by acid ions could be neglected, as the maximum value is close to reaching a plateau. In the last sample, 4 wt% and 5 wt% had similar values at one month of exposure. This could mean that small variations in the networks produce similar results.

Fig. 9 compares all the samples at the different time frames. It can be spotted that the influence is found during the month of acid attack. Finally, Fig. 10 depicts the influences of the percentage of carbon nanotubes and the time frames of acid attacks in the antenna bandwidth at different percentages of return loss. It is observed, in Fig. 10 b) and c) that as time passes the bandwidth seems to increase up to two weeks thereafter, it faces a huge decrement. This variation within weeks along with the variation in the return loss can also help to sense the ions penetrations before one month.

4. Conclusions

This study investigated the effects of acid attack in CNT/Polymer nanocomposites at various filler weight percentages using wireless measurements. Using a Vector Network Analyzer the scattering parameters were extracted in the frequency range of 3–6 GHz employing a microstrip antenna with a resonance frequency of 5 GHz. The contactless measurements were performed in an anechoic chamber with the specimens at zero days, one week, two weeks, and one month of acid exposure. Experimentally, it was found that acid diffusion alters the return and insertion loss results. With pristine epoxy, the acid attack alters the behaviours as early as one week. While as the percentage of Carbon Nanotubes increases the acid diffusion is delayed, the penetration of ions modifies the electrical properties of the CNT networks within the matrix. Thus, the acid influence is more significant in the one month specimens. Moreover, at 2 wt%, the largest variation between the control samples and one month of acid exposure samples was observed. This phenomenon was reduced until 5 wt% where minimal variation was observed. An idealized multi-scale modelling approach was implemented to study the potential alteration and its effects on the electrical conductivity, porosity, agglomeration, and the dielectric constant in the scattering parameters. It was found that the variation of electrical properties along with porosity volume produces return loss reduction at resonance frequency matching the experimental results. Thus, the two main events in an acid attack are the increase in the electrical conductivity and the generation of porosity around the surface of the nanocomposite.

CRediT authorship contribution statement

S. Tamayo-Vegas: Writing – original draft, Investigation, Formal analysis, Software, Investigation. **K. Lafdi:** Supervision, Project administration, Validation, Conceptualization, Methodology. **M. Elsdon:** Supervision, Formal analysis, Validation.

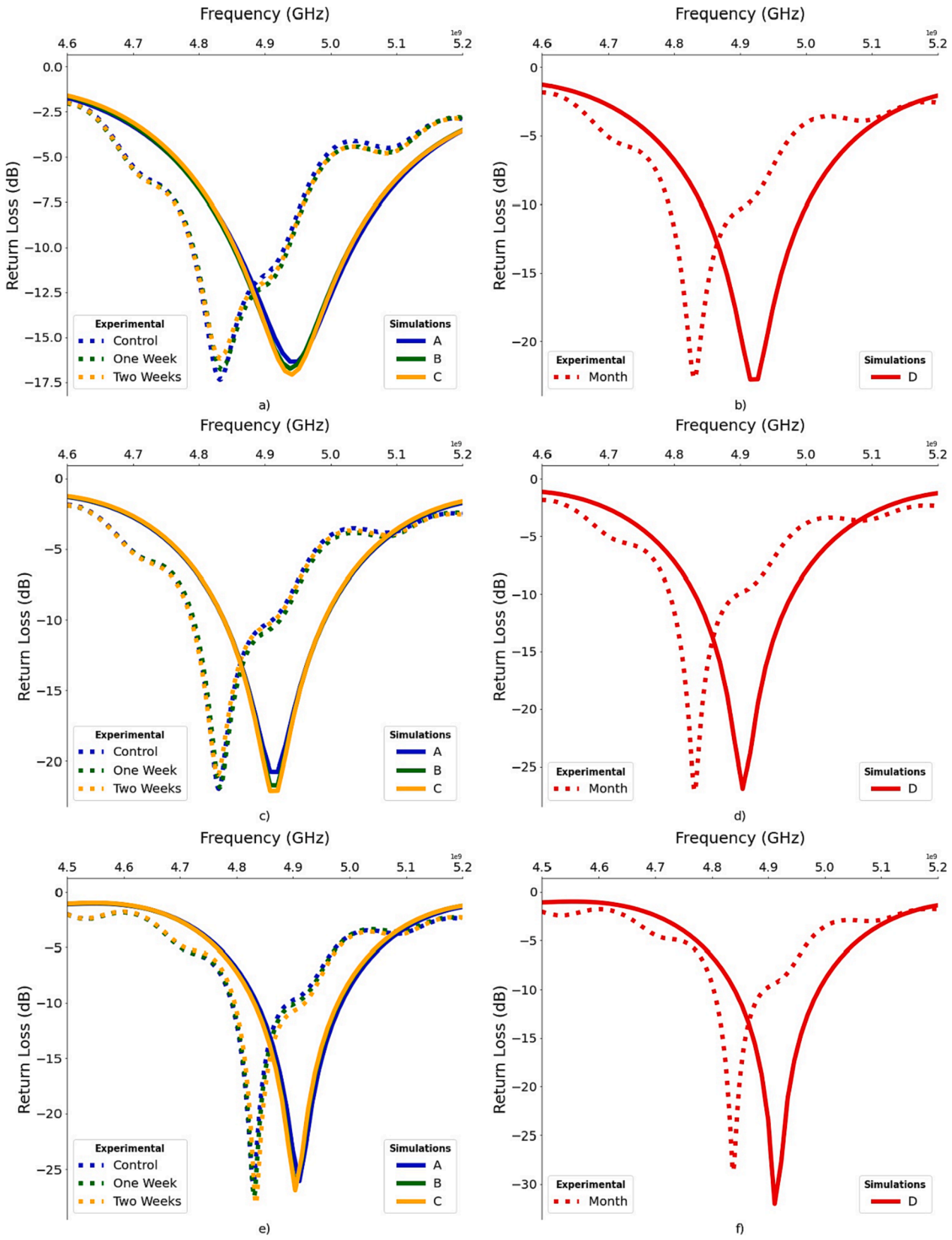

Fig. 8. Comparison of S11 curve experimental and numerical results after electrical percolation threshold a) 2 wt% one and two weeks. b) 2 wt% month. c) 4 wt% one and two weeks d) 4 wt% month e) 5 wt% one and two weeks f) 5 wt% month.

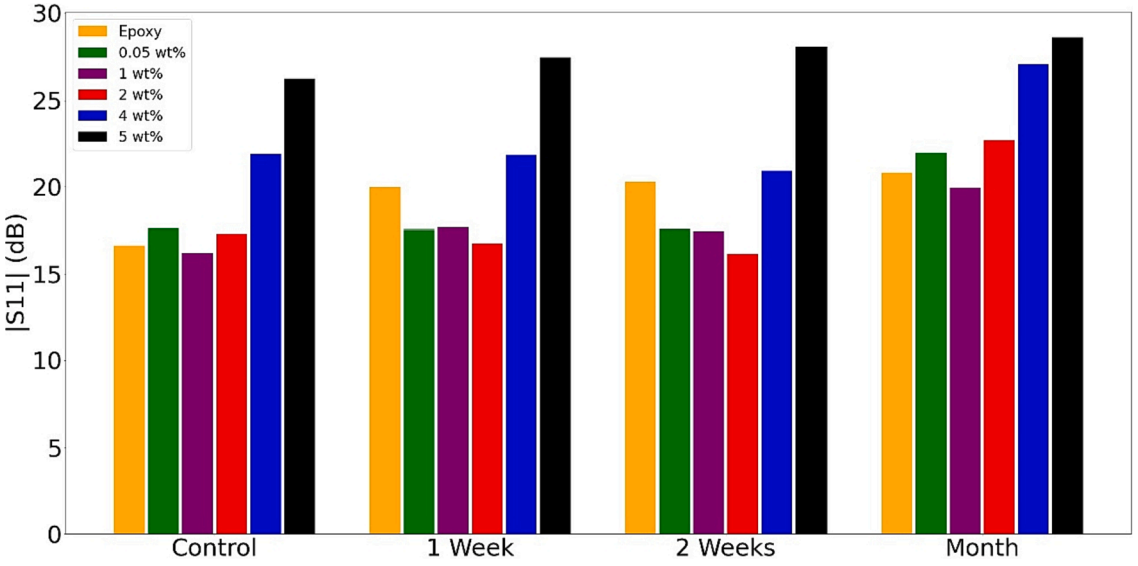

Fig. 9. Comparison of S11 Experimental Absolute Values at resonance Frequency.

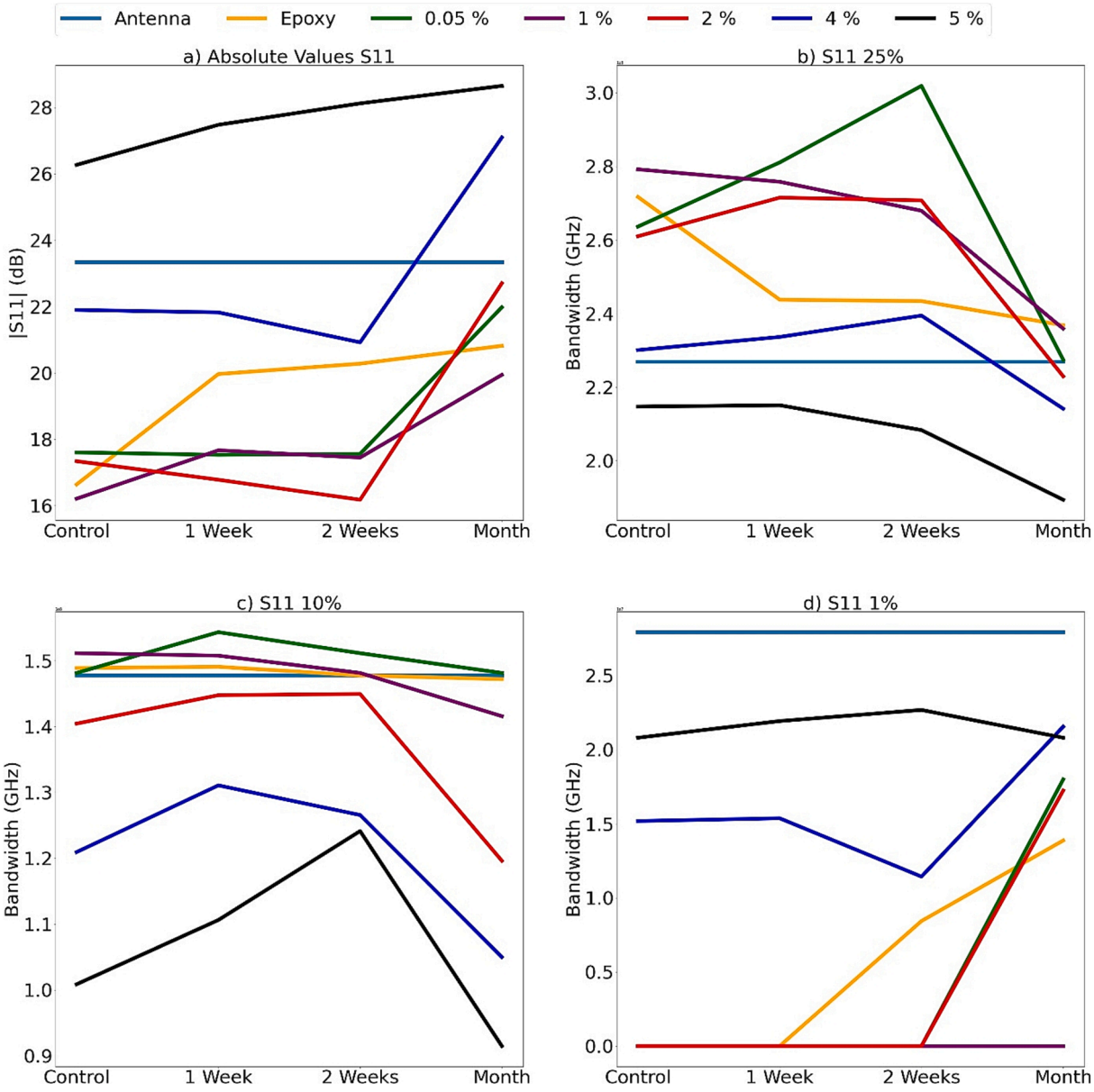

Fig. 10. Comparison of Acid influence on the samples of a) Absolute value of S11 b) bandwidth at 25 % c) bandwidth at 10 % d) bandwidth at 1%.

Declaration of Competing Interest

The authors declare that they have no known competing financial interests or personal relationships that could have appeared to influence the work reported in this paper.

Data availability

No data was used for the research described in the article.

References

[1] Shabaze M, Sahoo PK, Jagannatha Guptha VL. Multiscale material modelling and analysis of carbon fiber/MWCNT/ epoxy composites to predict effective elastic constants. Mater Today Proc 2019;19:521–7. https://doi.org/10.1016/j.matpr.2019.07.647.

[2] Khammassi S, Tarfaoui M. Influence of exfoliated graphite filler size on the electrical, thermal, and mechanical polymer properties. J Compos Mater 2020;54:3731–41. https://doi.org/10.1177/0021998320918639.

[3] El Moumen A, Tarfaoui M, Lafdi K, Benyahia H. Dynamic properties of carbon nanotubes reinforced carbon fibers/epoxy textile composites under low velocity impact. Compos Part B Eng 2017;125:1–8. https://doi.org/10.1016/j.compositesb.2017.05.065.

[4] Tamayo-Vegas S, Lafdi K. Experimental and modelling of temperature-dependent mechanical properties of CNT/polymer nanocomposites. Mater Today Proc 2022:1–8. https://doi.org/10.1016/j.matpr.2022.01.480.

[5] Tamayo-Vegas S, Muhsan A, Tarfaoui M, Lafdi K, Chang L. Effect of CNT additives on the electrical properties of derived nanocomposites (experimentally and numerical investigation). Mater Today Proc 2021:3–9. https://doi.org/10.1016/j.matpr.2021.09.361.

[6] Tarfaoui M, Lafdi K, Beloufa I, Daloia D, Muhsan A. Effect of graphene nano-additives on the local mechanical behavior of derived polymer nanocomposites. Polymers (Basel) 2018;10. https://doi.org/10.3390/polym10060667.

[7] El Moumen A, Tarfaoui M, Lafdi K. Computational homogenization of mechanical properties for laminate composites reinforced with thin filmmade of carbon nanotubes. Appl Compos Mater 2017;25:569–88. https://doi.org/10.1007/s10443-017-9636-2.

[8] Tarfaoui M, Lafdi K, El Moumen A. Mechanical properties of carbon nanotubes based polymer composites. Compos Part B Eng 2016;103:113–21. https://doi.org/10.1016/j.compositesb.2016.08.016.

[9] Khammassi S, Tarfaoui M. Micromechanical characterization of Carbon Black reinforced adhesive nanocomposite using micro indentation. Mater Today Proc 2022;52:222–6. https://doi.org/10.1016/j.matpr.2021.11.345.

[10] Khammassi S, Tarfaoui M, Qureshi Y, Benyahia H. Mechanical properties of graphene nanoplatelets reinforced epikote 828 under dynamic compression. Mech Mater 2021;158:103873. https://doi.org/10.1016/j.mechmat.2021.103873.

[11] Tanks JD, Arao Y, Kubouchi M. Diffusion kinetics, swelling, and degradation of corrosion-resistant C-glass/epoxy woven composites in harsh environments. Compos Struct 2018;202:686–94. https://doi.org/10.1016/j.compstruct.2018.03.078.

[12] Pradyawong P, Kubouchi M, Aoki S, Sakai T. The study of HCL penetration behavior inside of an unsaturated polyester resin under temperature gradient to simulate the accidental roof failure of FRP outdoor storage tank containing high concentration HCL solution. ICCM Int Conf Compos Mater 2015:2015-July.

[13] Pradchar P, Aoki S, Kubouchi M, Sakai T. The effect of cyclic temperature of sulfuric acid on flexural property of matrix resin for FRP storage. J Chem Eng Japan 2015;48:670–7. https://doi.org/10.1252/jcej.14we320.

[14] Liu C, Lafdi K, Chinesta F. Durability sensor using low concentration carbon nano additives. Compos Sci Technol 2020;195:108200. https://doi.org/10.1016/j.compscitech.2020.108200.

[15] Yu YT, Pochiraju K. Three-dimensional simulation of moisture diffusion in polymer composite materials. Polym - Plast Technol Eng 2003;42:737–56. https://doi.org/10.1081/PPT-120024993.

[16] Liu, C.; Lafdi, K. ENVIRONMENTAL MONITORING OF COMPOSITE DURABILITY USE MULTIPLE SENSING TECHNOLOGIES. In Proceedings of the The Composites and Advanced Materials Expo.; Dallas, 2018.

[17] Gomasang P, Kawahara K, Yasuraoka K, Maruyama M, Ago H, Okada S, et al. A novel graphene barrier against moisture by multiple stacking large-grain graphene. Sci Rep 2019;9:1–10. https://doi.org/10.1038/s41598-019-40534-5.

[18] Liu C, Fang Q, Lafdi K. Novel wireless sensing design for composite durability study. Compos Commun 2020;22:100511. https://doi.org/10.1016/j.coco.2020.100511.

[19] Tamayo-Vegas S, Lafdi K. A literature review of non-contact tools and methods in structural health monitoring. Eng Technol Open Access J 2021;4. https://doi.org/10.19080/etoaj.2021.04.555626.

[20] Duroc Y, Tedjini S. RFID: a key technology for Humanity. Comptes Rendus Phys 2018;19:64–71. https://doi.org/10.1016/j.crhy.2018.01.003.

[21] M.S, Kranz, B.A, English, Whitley, M.R. RFID-Inspired Wireless Microsensors for Structural Health Monitoring. In Proceedings of the IEEE Aerospace Conference Proceedings; IEEE, 2016; Vol. 2016, pp. 1–7.

[22] Kassal P, Steinberg MD, Steinberg IM. Wireless chemical sensors and biosensors: a review. Sens Actua B Chem 2018;266:228–45. https://doi.org/10.1016/j.snb.2018.03.074.

[23] Duan KK, Cao SY. Emerging RFID technology in structural engineering – a review. Structures 2020;28:2404–14. https://doi.org/10.1016/j.istruc.2020.10.036.

[24] La Saponara V. Environmental and chemical degradation of carbon/epoxy and structural adhesive for aerospace applications: Fickian and anomalous diffusion. Arrhenius kinetics *Compos Struct* 2011;93:2180–95. https://doi.org/10.1016/j.compstruct.2011.03.005.

[25] Mahmoud MK, Tantawi SH. Effect of strong acids on mechanical properties of glass/polyester GRP pipe at normal and high temperatures. Polym - Plast Technol Eng 2003;42:677–88. https://doi.org/10.1081/PPT-120023102.

[26] Abastari; Sakai, T.; Sembokuya, H.; Kubouchi, M.; Tsuda, K. Study on permeation behavior and chemical degradation of PA66 in acid solution. *Polym. Degrad. Stab.* **2007**, *92*, 379–388, doi:10.1016/j.polymdegradstab.2006.12.002.

[27] Soodmand S, Brown TWC. Inductively coupled small self resonant coil (SSRC) reader antennas for HF RFID applications. AEU - Int J Electron Commun 2017;78:32–40. https://doi.org/10.1016/j.aeue.2017.05.019.

[28] Loh KJ, Lynch JP, Kotov NA. Inductively coupled nanocomposite wireless strain and pH sensors. Smart Struct Syst 2008;4:531–48. https://doi.org/10.12989/sss.2008.4.5.531.

[29] Materer N, Field P, Ley N, Soufiani AR, Scott D, Ley T, et al. Passive wireless detection of corrosive salts in concrete using wire-based triggers. J Mater Civ Eng 2013;26. https://doi.org/10.1061/(asce)mt.1943-5533.0000881.

[30] Khalifeh R, Yasri MS, Lescop B, Gallee F, Diler E, Thierry D, et al. Development of Wireless and Passive Corrosion Sensors for Material Degradation Monitoring in Coastal Zones and Immersed Environment. IEEE J Ocean Eng 2016;41:776–82. https://doi.org/10.1109/JOE.2016.2572838.

[31] Singh R, Singh E, Nalwa HS. Inkjet printed nanomaterial based flexible radio frequency identification (RFID) tag sensors for the internet of nano things. RSC Adv 2017;7:48597–630. https://doi.org/10.1039/c7ra07191d.

[32] Zhu R, Desroches M, Yoon B, Swager TM. Wireless oxygen sensors enabled by Fe (II)-polymer wrapped carbon nanotubes. ACS Sensors 2017;2:1044–50. https://doi.org/10.1021/acssensors.7b00327.

[33] Lee JS, Oh J, Jun J, Jang J. Wireless Hydrogen Smart Sensor Based on Pt/Graphene-immobilized radio-frequency identification tag. ACS Nano 2015;9:7783–90. https://doi.org/10.1021/acsnano.5b02024.

[34] E, Abad, F, Palacio, M, Nuin, A.G, Zárate, A, de; Juarros, J.M, Gómez, S, Marco, RFID smart tag for traceability and cold chain monitoring of foods: Demonstration in an intercontinental fresh fish logistic chain. *J. Food Eng.* **2009**, *93*, 394–399, doi:10.1016/j.jfoodeng.2009.02.004.

[35] Alfian G, Rhee J, Ahn H, Lee J, Farooq U, Ijaz MF, et al. Integration of RFID, wireless sensor networks, and data mining in an e-pedigree food traceability system. J Food Eng 2017;212:65–75. https://doi.org/10.1016/j.jfoodeng.2017.05.008.

[36] Ghaani M, Cozzolino CA, Castelli G, Farris S. An overview of the intelligent packaging technologies in the food sector. Trends Food Sci Technol 2016;51:1–11. https://doi.org/10.1016/j.tifs.2016.02.008.

[37] Bibi F, Guillaume C, Gontard N, Sorli B. A review: RFID technology having sensing aptitudes for food industry and their contribution to tracking and monitoring of food products. Trends Food Sci Technol 2017;62:91–103. https://doi.org/10.1016/j.tifs.2017.01.013.

[38] Fiddes LK, Chang J, Yan N. Electrochemical detection of biogenic amines during food spoilage using an integrated sensing RFID tag. Sens Actua, B Chem 2014;202:1298–304. https://doi.org/10.1016/j.snb.2014.05.106.

[39] Potyrailo RA, Nagraj N, Tang Z, Mondello FJ, Surman C, Morris W. Battery-free radio frequency identification (RFID) sensors for food quality and safety. J Agric Food Chem 2012;60:8535–43. https://doi.org/10.1021/jf302416y.

[40] A, Nasir, B.H, Soong, EnvironSense: An integrated system for urban sensing using RFID based WSN's. *IEEE Reg. 10 Annu. Int. Conf. Proceedings/TENCON* **2009**, 1–5, doi:10.1109/TENCON.2009.5396076.

[41] Hoque MA, Azad M, Ashik-Uz-Zaman M. IoT and Machine Learning Based Smart Garbage Management and Segregation Approach for Bangladesh. ICIET 2019–2nd Int. Conf. Innov. Eng Technol 2019;23–24. https://doi.org/10.1109/ICIET48527.2019.9290551.

[42] Pang Y, Lodewijks G. The application of RFID technology in large-scale dry bulk material transport system monitoring. EESMS 2011–2011 IEEE Work. Environ Energy Struct Monit Syst Proc 2011;5–9. https://doi.org/10.1109/EESMS.2011.6067043.

[43] C, Ma, Y, Wang, G, Ying, The pig breeding management system based on RFID and WSN. *Proc. - 4th Int. Conf. Inf. Comput. ICIC 2011* **2011**, 30–33, doi:10.1109/ICIC.2011.133.

[44] Fiddes LK, Yan N. RFID tags for wireless electrochemical detection of volatile chemicals. Sens Actua, B Chem 2013;186:817–23. https://doi.org/10.1016/j.snb.2013.05.008.

[45] Kassal P, Kim J, Kumar R, De Araujo WR, Steinberg IM, Steinberg MD, et al. Smart bandage with wireless connectivity for uric acid biosensing as an indicator of wound status. Electrochem commun 2015;56:6–10. https://doi.org/10.1016/j.elecom.2015.03.018.

[46] Rohokale VM, Prasad NR, Prasad R. A cooperative Internet of Things (IoT) for rural healthcare monitoring and control. *2011 2nd Int.* Conf Wirel Commun Veh Technol Inf Theory Aerosp Electron Syst Technol Wirel VITAE 2011. https://doi.org/10.1109/WIRELESSVITAE.2011.5940920.

[47] Lin CC, Lin PY, Lu PK, Hsieh GY, Lee WL, Lee RG. A healthcare integration system for disease assessment and safety monitoring of dementia patients. IEEE Trans Inf Technol Biomed 2008;12:579–86. https://doi.org/10.1109/TITB.2008.917914.

[48] Kim SC, Jeong YS, Park SO. RFID-based indoor location tracking to ensure the safety of the elderly in smart home environments. Pers Ubiquitous Comput 2013; 17:1699–707. https://doi.org/10.1007/s00779-012-0604-4.
[49] Amendola S, Lodato R, Manzari S, Occhiuzzi C, Marrocco G. RFID technology for IoT-based personal healthcare in smart spaces. IEEE Internet Things J 2014;1: 144–52. https://doi.org/10.1109/JIOT.2014.2313981.
[50] Jayawardana D, Kharkovsky S, Liyanapathirana R. Measurement system with a RFID tag antenna mounted on structural members for infrastructure health monitoring. Conf Rec - IEEE Instrum Meas Technol Conf Proc 2015;2015:7–12. https://doi.org/10.1109/I2MTC.2015.7151231.
[51] Marindra AMJ, Tian GY. Chipless RFID Sensor tag for metal crack detection and characterization. IEEE Trans Microw Theory Tech 2018;66:2452–62. https://doi.org/10.1109/TMTT.2017.2786696.
[52] Merilampi S, Björninen T, Ukkonen L, Ruuskanen P, Sydänheimo L. Embedded wireless strain sensors based on printed RFID tag. Sens Rev 2011;31:32–40. https://doi.org/10.1108/02602281111099062.
[53] Matheus FK, Frank PM, Marcelo FB, Thomas GRC. RFID wireless system for detection of water in the annulus of a flexible pipe. Mar Struct 2020;72:102776. https://doi.org/10.1016/j.marstruc.2020.102776.
[54] Babar AA, Manzari S, Sydanheimo L, Elsherbeni AZ, Ukkonen L. Passive UHF RFID Tag for Heat Sensing Applications. IEEE Trans Antennas Propag 2012;60:4056–64. https://doi.org/10.1109/TAP.2012.2207045.
[55] Liu C, Sergeichev I, Akhatov I, Lafdi K. CNT and polyaniline based sensors for the detection of acid penetration in polymer composite. Compos Sci Technol 2018;159: 111–8. https://doi.org/10.1016/j.compscitech.2018.02.028.
[56] Ghodgaonkar DK, Varadan VV, Varadan VK. A free-space method for measurement of dielectric constants and loss tangents at microwave frequencies. IEEE Trans Instrum Meas 1989;38:789–93. https://doi.org/10.1109/19.32194.
[57] Ek-Weis J, Eriksson A, Idda T, Olofsson N, Campbell EEB. Radio-frequency characterization of varactors based on carbon nanotube arrays. Proc Inst Mech Eng Part N J Nanoeng Nanosyst 2008;222:111–5. https://doi.org/10.1243/17403499JNN122.
[58] Katsounaros A, Rajab KZ, Hao Y, Mann M, Milne WI. Microwave characterization of vertically aligned multiwalled carbon nanotube arrays. Appl Phys Lett 2011;98: 1–4. https://doi.org/10.1063/1.3592263.
[59] A, Katsounaros, K.Z, Rajab, Y, Hao, M, Mann, W.I, Milne, X-band characterization of multi-walled carbon nanotube films. *Proc. - 2011 Int. Conf. Electromagn. Adv. Appl. ICEAA'11* **2011**, 516–519, doi:10.1109/ICEAA.2011.6046394.
[60] S, Thomas, R, Thomas, A.K, Zachariah, R.K, Mishra, *Spectroscopic Methods for Nanomaterials Characterization*; 2017; Vol. 2; ISBN 9780323461467.
[61] Afsar MN, Afsar MN, Birch JR, Clarke RN, Chantry GW. The measurement of the properties of materials. Proc IEEE 1986;74:183–99. https://doi.org/10.1109/PROC.1986.13432.
[62] Tamayo-Vegas S, Muhsan A, Liu C, Tarfaoui M, Lafdi K. The effect of agglomeration on the electrical and mechanical properties of polymer matrix nanocomposites reinforced with carbon nanotubes. Polymers (Basel) 2022;14:1–18.